THE ASTROPHYSICAL JOURNAL, 328:334–343, 1988 May 1

HEATING-RELATED FLOWS IN COOL SOLAR LOOPS

J. A. KLIMCHUK[1] AND J. T. MARISKA
E. O. Hulburt Center for Space Research, Naval Research Laboratory

Received 1987 August 3; accepted 1987 October 20

ABSTRACT

We have investigated the effects of spatial and temporal variations in the heating of cool-type solar loop models. In contrast to hot loops, these cool loops have temperature gradients that are everywhere shallow and maximum temperatures that are well below 10^6 K. The results of our numerical simulations show that spatial asymmetries in the energy input to cool loops will produce steady state, end-to-end flows. Velocities exceeding 20 km s^{-1} are possible. In no case, however, is the downflowing leg appreciably faster or appreciably brighter than the upflowing leg (at a given temperature), and no significant Dopper shift would be seen from an unresolved loop. Other simulations show that symmetric, but sudden, reductions in the energy input can also produce downflows of large velocity. These flows are transient, and because they arise from cooling of the plasma, the greatest velocities (>4 km s^{-1}) are restricted to temperatures below 5×10^4 K. We conclude from these results that spatial and temporal heating variations of the types considered here are unable to explain the net redshifts observed in emission lines formed near 10^5 K on the Sun.

Subject headings: Sun: atmosphere — Sun: atmospheric motions

I. INTRODUCTION

A variety of rocket and satellite missions have now established the existence of a general downflow into both quiet and active areas on the Sun. Ultraviolet emission lines formed at temperatures near 10^5 K in the transition region exhibit disk-averaged redshifts of ~ 7 km s^{-1} in the quiet Sun (Dere, Bartoe, and Brueckner 1984, 1986; Roussel-Dupre and Shine 1982; Doschek, Feldman, and Bohlin 1976; Shine 1985) and ~ 12 km s^{-1} in active regions (Feldman, Cohen, and Doschek 1982; Dere 1982; Brueckner 1981; Klimchuk 1986, 1987). As a rule, the redshifts are greater where the magnetic field is enhanced (e.g., the network) and in observations made closer to disk center. We thus expect the vertical component of downflow in magnetic regions to be somewhat greater than the disk-averaged redshifts.

Several different suggestions have been made as to the origin of the observed redshifts. One idea involves the injection of cool ($\sim 10^4$ K) spicular material into the corona, which then heats and falls to the surface at a higher temperature (Pneuman and Kopp 1978; Athay and Holzer 1982). Indeed, crude estimates of the global mass fluxes in the spicular and UV-emitting material seem to agree. No strong conclusions can be drawn from this apparent agreement, however, since the flux estimates are each uncertain by a factor of at least 3.

Other ideas have considered the effects of spatial and temporal variations in the heating of existing hot material within magnetically closed regions of the atmosphere. Boris and Mariska (1982), Mariska and Boris (1983), Craig and McClymont (1986), McClymont and Craig (1986, 1987), and Mariska (1987*b*, *c*) studied coronal loop models and found that steady state, end-to-end flows will occur if the energy input is distributed asymmetrically about the loop apex. While these models can reproduce many aspects of the observations, including the net redshifts, they tend to require loop lengths that are very short ($\sim 10^3$ km) or pressures that are smaller than observed ($\sim 10^{-2}$ dyn cm^{-2}).

Mariska *et al.* (1982) and Mariska (1987*a*) found that symmetric, but sudden, reductions in the energy input to hot loops can also produce downflows of the correct magnitude. The problem here is that the emission at 10^5 K is much too faint to be important. Thus, both scenarios involving heating variations in hot loops fall short in explaining all aspects of the solar observations.

Another class of loop model, called cool loops, has recently been emphasized in the literature (Antiochos and Noci 1986; Woods, Holzer, and MacGregor 1987*a*; McClymont 1987; Martens and Kuin 1982; Hood and Priest 1979). Temperature gradients are everywhere shallow in cool loops, and, depending on the functional forms of the energy input and radiative losses, the maximum temperature is of order 10^5 K. By comparison, hot loops have steep temperature gradients in the transition region and reach a maximum temperature of order 10^6 K.

Because of their temperature structure, cool loops emit much more strongly at temperatures near 10^5 K than do hot loops. It is speculated that they may be an important component of the solar atmosphere and that they may explain the lower temperature, negative slope end of the observed emission measure curve, where hot loop models are substantially inadequate (Antiochos and Noci 1986; Dowdy, Rabin, and Moore 1986). Here we explore the hypothesis that cool loops can also explain the observed redshifts.

Because cool loops are a relatively new topic in solar physics, their dynamics is only now being seriously investigated (Klimchuk and Mariska 1987; McClymont 1987). As an obvious extension of the hot loop modeling described above, we have examined the dependence of cool loop models on both spatial and temporal variations in the energy input. Specifically, we have simulated the response of initially static cool loops to changes in the energy input. As for hot loops, it is found that spatially asymmetric changes produce a final steady state that is dynamic and that spatially symmetric changes

[1] NRC-NRL Cooperative Research Associate. Current address: Center for Space Science and Astrophysics, Stanford University.

produce a final state that is static. We discuss these two cases separately in §§ IV and V. The numerical model used for this investigation is described in § II. In § III we discuss some general properties of cool loop equilibria, paying particular attention to the relationship between structure and energy input. Finally, in § VI we review and comment on our results.

II. THE MODEL

The numerical model we use to study the behavior of cool loop atmospheres was developed at the Naval Research Laboratory initially for studying hot loops (e.g., Mariska *et al.* 1982; Klimchuk, Antiochos, and Mariska 1987). The computer code solves the one-dimensional, time-dependent equations of mass, momentum, and energy transport for a fully ionized solar plasma confined within a rigid magnetic flux tube:

$$\frac{\partial \rho}{\partial t} + \frac{\partial}{\partial s}(\rho v) = 0 , \tag{1}$$

$$\frac{\partial}{\partial t}(\rho v) + \frac{\partial}{\partial s}(\rho v^2) = \rho g_{\parallel} - \frac{\partial P}{\partial s} , \tag{2}$$

and

$$\frac{\partial E}{\partial t} + \frac{\partial}{\partial s}[(E + P)v] = \rho v g_{\parallel} + \frac{\partial}{\partial s}\left(\kappa_0 T^{5/2}\frac{\partial T}{\partial s}\right) - n_e n_p \Lambda(T) + \epsilon , \tag{3}$$

where

$$E = \frac{1}{2}\rho v^2 + \frac{P}{\gamma - 1} . \tag{4}$$

Here, t is the time; s is the spatial coordinate along the axis of the tube; ρ, P, T, and v are the total mass density, total pressure, temperature, and bulk velocity, respectively; n_e and n_p are the number densities of electrons and protons; $g_{\parallel}$ is the gravitational acceleration parallel to the tube; κ_0 is the coefficient of thermal conductivity; and γ is the ratio of specific heats, taken to be 5/3 throughout the atmosphere. The term involving $\Lambda(T)$ describes the rate of energy loss due to radiation, and ϵ describes the rate of energy input due to mechanical heating of unknown origin. For these calculations we assume that the energy input depends only on position, density, and time. We further assume that the heating mechanism does not impart momentum directly to the plasma, though this may be a poor approximation for certain forms of wave heating (see § VI).

The system of equations is completed with the ideal gas law,

$$P = nkT , \tag{5}$$

where n is the total number density and k is Boltzmann's constant.

We solve these equations on a finite-difference grid using time-step splitting. Convective terms are treated explicitly using a flux-corrected transport (FCT) algorithm (Book, Boris, and Hain 1975), and thermal conduction is treated implicitly to maintain numerical stability. Because of the shallow gradients characteristic of cool loop atmospheres, a computational cell size ranging from 100 km in the chromosphere to 10 km in the overlying regions provides adequate spatial resolution.

The flux tube geometry is that of a semicircular loop attached to long, straight chromospheric legs. For the short loop we consider first the loop radius, and therefore its height, is 1.5×10^3 km. A taller loop of radius 6×10^3 km is considered in § V*b*. The chromospheric legs range in size from 4×10^3 km for the uniform heating simulations to 8×10^3 km for the asymmetric heating simulations. In all cases the cross-sectional area of the flux tube is constant.

The detailed radiative loss properties of the lower transition region are not well understood at this time. While it is clear that the atmosphere below $\sim 6 \times 10^4$ K is not optically thin in some transitions, the degree to which optical depth effects are important is not obvious. We choose to follow the suggestion of McClymont and Canfield (1983) that the radiative loss curve between 2×10^4 and 10^5 K obeys the approximate power law

$$\Lambda(T) = \Lambda_0 T^3 . \tag{6}$$

A value for Λ_0 of 6.46×10^{-37} ergs cm^3 s^{-1} K^{-3} gives agreement with Raymond's (1979) optically thin loss curve at 10^5 K. Athay (1986*a*) has recently argued that the optical depth effects implicit in equation (6) may be overemphasized and that the T^3 dependence may be too strong. In any event, it is possible, if not probable, that the dependence is stronger than T^2 above 3×10^4 K.

The detailed temperature structure of the solar chromosphere is determined almost entirely by the radiative properties of the chromospheric plasma (Athay 1985, 1986*b*). A plateau occurs near 6500 K due to the strong temperature dependence of hydrogen ionization and the availability of free electrons to excite Ca II and Mg II transitions responsible for most of the radiation. As a result, the chromosphere behaves something like a thermostat, maintaining uniform temperatures over a wide range of pressures and energy inputs. A second, narrower temperature plateau occurs near 2×10^4 K due to the escape of Lyα photons.

For our model we have adopted an isothermal chromosphere corresponding to a single temperature plateau. As in our earlier hot loop simulations (Klimchuk, Antiochos, and Mariska 1987) we assume a value of 2×10^4 K, corresponding to the upper plateau. In retrospect, we see that a choice of 6500 K may have been more appropriate, since the dynamical response of the chromosphere is determined mostly by the gravitational scale height of the lower, much thicker plateau. Our basic conclusions should not be adversely affected, however (2×10^4 K remains the best choice for hot loop models, since for these models thermal conduction is important and should approximately vanish at the upper plateau). As discussed in Klimchuk, Antiochos, and Mariska (1987), the model chromosphere is kept nearly isothermal by introducing a precipitous decrease in the radiative loss curve for temperatures below 2×10^4 K; whenever the plasma cools to a lower temperature, the radiative losses are severely suppressed and the atmosphere reheats.

III. STATIC EQUILIBRIA

a) Basic Properties

It is worthwhile to now review some of the basic properties of static cool loop equilibria. Further details can be found in Antiochos and Noci (1986) and in Woods, Holzer, and MacGregor (1987*a*). We first consider a loop that is heated symmetrically by an energy input that is uniform in space. Figure 1 shows the equilibrium profiles of temperature, density, and pressure that result for a quiet-Sun base pressure (at the top of the chromosphere) of 0.2 dyn cm^{-2} (Mariska 1986). The apex temperature is 7.5×10^4 K.

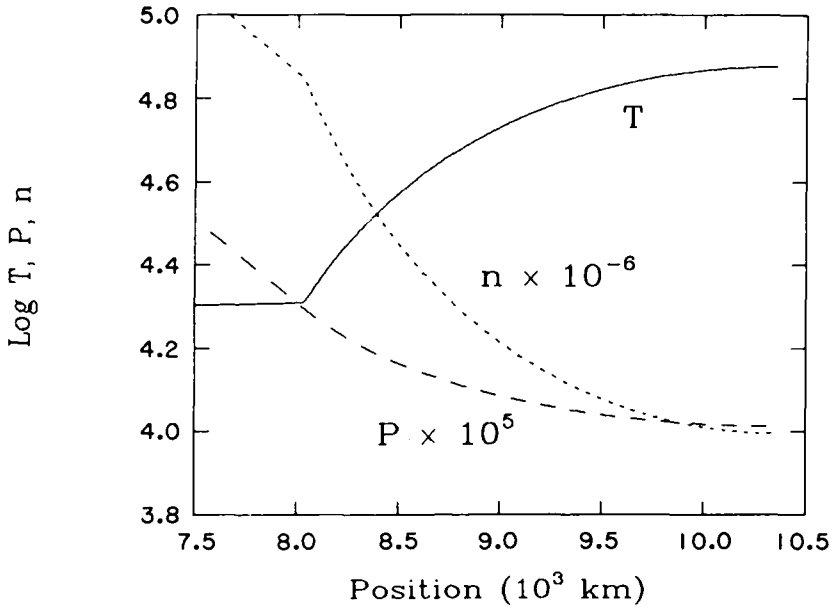

FIG. 1.—The static equilibrium structure of a uniformly heated short loop of radius 1.5×10^3 km: temperature (K), total pressure (dyn cm^{-2}), and total number density (cm^{-3}) are plotted as a function of position along the loop axis. Only half of the loop is shown because of symmetry. The apex is located at position 1.04×10^4 km and the base (top of chromosphere) at position 8.0×10^3 km. Please note that the vertical scale is logarithmic.

Unlike hot loops, whose temperatures rise first abruptly in the transition region and then very minimally in the corona, static cool loops have temperatures that increase both gradually and steadily throughout. This contrast is related to the fundamental difference in energy balance in these two types of atmospheres. In hot loops, thermal conduction plays an important role transporting energy from the corona down to the transition region; steep temperature gradients are necessary at the lower temperatures to maintain the large conductive flux. In cool loops, thermal conduction is relatively unimportant, and there is everywhere a local balance between radiation and energy input.

In a uniformly heated cool loop, radiation is also uniform, and the temperature increases with height in order to offset the effects of decreasing, gravitationally stratified density [$n^2\Lambda(T) = $ constant]. If the heating decreases with height, the temperature rises less quickly, and the heating increases with height, the temperature rises more quickly. For radiative loss curves having a weaker dependence than T^2, the heating must not only decrease with height, but it must decrease sufficiently rapidly; otherwise, cool equilibria are not possible (Woods, Holzer, and MacGregor 1987*a*).

The maximum temperature attainable by a cool equilibrium under the conditions of our model is 10^5 K, the temperature at which the constant pressure form of the loss curve, $\Lambda(T)/T^2$, first has a negative slope. Beyond this a temperature increase cannot offset a density decrease, and the radiation is necessarily reduced. Energy balance is impossible with uniform heating and it is difficult with heating that decreases with height, since $\Lambda(T)$ is itself negatively sloped beyond 10^5 K.

The maximum temperature in our model places an upper limit on the possible height of the loop. With heating that is uniform in space, the maximum height is 2×10^3 km, and with heating that is constant per unit mass, the maximum height is 8×10^3 km (Antiochos and Noci 1986). Greater temperatures and heights are possible for different loss curves and heating functions, however (Woods, Holzer, and MacGregor 1978*a*). There is no limit to the height of hot loops.

The gravitational scale height of a hot loop is generally large compared to its geometric height, and consequently the pressure is nearly constant. The same is not true of cool loops, on the other hand, which have a noticeable pressure stratification. In Figure 1, for example, the pressure decreases by a factor of 2 from the base to the apex. The density decreases even more because of the temperature increase required for energy balance.

b) Dependence on Energy Input

We now examine the relationship between atmospheric structure and energy input in more detail. It will be assumed here that the energy input depends only on position.

Thermal conduction is fully ignorable for the cool loops we are now considering, and the static energy equation reduces to

$$\Lambda_0 n_e^2 T^3 = \epsilon \,, \tag{7}$$

where we have taken $n_e = n_p = n/2$. With the aid of the ideal gas law, this can be rewritten as

$$T = \frac{4k^2\epsilon}{\Lambda_0 P^2} \,, \tag{8}$$

showing that temperature is directly proportional to energy input. In regions of uniform pressure, the temperature and energy input profiles will therefore have similar form. Local deviations in heating should produce local deviations in temperature.

The static momentum equation is simply

$$\frac{dP}{dz} = -m_p n_e g \,, \tag{9}$$

where m_p is the proton rest mass, z is the vertical spatial coordinate, increasing upward, and g is a positive constant. The z

coordinate should not be confused with the curvilinear coordinate, s, in equations (1)–(3). Substituting for n_e using the ideal gas law and equation (8) we get

$$\frac{dP}{dz} = -\frac{m_p g \Lambda_0 P^3}{8k^3 \epsilon}. \tag{10}$$

The pressure at any height, including the apex, h, can then be easily obtained by integrating upward from the base (top of chromosphere):

$$P(h) = P_0\left[1 + \frac{2}{H_0}\int_{z_0}^{h}\frac{dz}{f(z)}\right]^{-1/2}, \tag{11}$$

where P_0 is the base pressure,

$$H_0 \equiv \frac{2kT_0}{m_p g} \tag{12}$$

is the gravitational scale height at the base, and

$$f(z) \equiv \frac{\epsilon(z)}{\epsilon_0} \tag{13}$$

is the heating function normalized to its base value. Equation (11) is a simplified form of the more general equation derived by Antiochos and Noci (1986, their eq. [17]).

We see from equation (11) that the pressure at any given height in a cool loop depends on the heating at all levels below, but not on the heating above. It also depends on the base pressure, which is given uniquely by the base heating (and base temperature) according to equation (8). This result contrasts with hot loops, where, because of thermal conduction, the pressure at each height depends on the heating at *all* other locations throughout the loop.

In order for a cool loop to be in static equilibrium, the apex pressure given by equation (11) must be the same for both of the loop legs. Otherwise, an unbalanced pressure gradient would exist at the top, where gravity exerts no force parallel to the loop axis. Assuming equal base pressure at the two footpoints, pressure equilibrium at the apex is trivially satisfied in the case of symmetric heating. For asymmetric heating, on the other hand, a pressure imbalance will drive a flow from the higher pressure, more strongly heated, leg to the lower pressure, less strongly heated, leg. Any equilibrium must necessarily be dynamic.

IV. ASYMMETRIC HEATING

In principle, one could study the dynamic equilibria that result from asymmetric heating by solving the steady state equations directly. Instead, we obtain the steady state solution by applying asymmetric heating to an initially static cool loop and allowing it to evolve asymptotically to a final equilibrium. In that way we can also examine the intermediate, nonequilibrium states that might be expected to occur on the Sun.

a) Localized Energy Source

In the first of our simulations we consider the effects of adding energy locally to only one side of a loop. Beginning with the static atmosphere of Figure 1, and without altering the uniform background heating, we gradually turn on an energy source concentrated halfway up one of the legs. It has a Gaussian distribution with an e^{-1} half-width of 500 km and a central amplitude equal to 50% of the background heating rate. The source is activated over a period of 100 s, after which time the asymmetric heating is held constant. Figure 2 indicates the response of the loop to the additional heating: temperature and velocity profiles are shown for selected times both before and after the source is turned on. (Note that this and following temperature plots in this paper are plotted linearly, rather than logarithmically, as is usually done for hot loops.)

Temperatures rise quickly in the region of the additional heating, and within 300 s a bump appears on the temperature profile having a similar shape and magnitude to the energy source itself. This is expected from equation (8), since pressure is roughly uniform over the region and the flows are not large enough to significantly affect the equilibrium structure. Elsewhere in the loop the temperatures are essentially unchanged, reflecting the fact that the energy input in those regions is also unchanged.

Mass motions produced by the additional heating are initially away from the source in both directions. This is only a short term response to the local pressure increase, however, and within 200 s the atmosphere adjusts to set up a unidirectional flow away from the footpoint on the more strongly heated side. Flow velocities gradually increase until an approximate steady state is achieved at $t = 1000$ s. After this time, until the simulation is terminated at $t = 7000$ s, the atmosphere is virtually constant. A maximum velocity of 5 km s^{-1} occurs in the upflowing leg, at the approximate location of the energy source. The striking similarity between the equilibrium velocity and temperature profiles is a direct consequence of mass conservation in a region of slowly varying pressure.

The flow produced here is too slow to explain the net redshifts observed on the Sun, regardless of the emission properties of the plasma. McClymont and Craig (1987) and Mariska (1987*b*, *c*) have recently shown that in asymmetrically heated hot loops the flow velocities are greatest when the energy input is highly concentrated in a narrow region close to the chromosphere. To determine whether this is also true of cool loops we have performed a second simulation, similar to the first, but with the Gaussian energy source centered only 300 km above the base and having a half-width of only 100 km. The central amplitude is 200% of the background heating rate, which is close to the upper limit allowed by the cool state (for greater amplitudes the temperature rises above 10^5 K and the atmosphere quickly evolves to a 10^6 K hot state).

The effects of this type of heating are qualitatively similar to before. Temperatures become enhanced at the source, this time forming a spike on the profile rather than a bump, and a steady state flow is produced carrying material away from the more strongly heated leg. At no time do the velocities exceed 3 km s^{-1}, however. We conclude that neither the location nor the concentration of the energy source is a strong factor in determining the maximum flow speed in cool loops.

b) Exponential Form

In both of these simulations the energy content of the source is small compared to the spatially integrated background heating of the loop. Consequently, the left leg receives only $\sim 20\%$ more total energy than the right leg. To determine whether an asymmetry in the total amount of heating is important for driving flows, we have considered a completely different form for the heating profile. Instead of a localized energy source, we introduce a component of heating that decreases exponentially along the axis of the loop, from one footpoint to

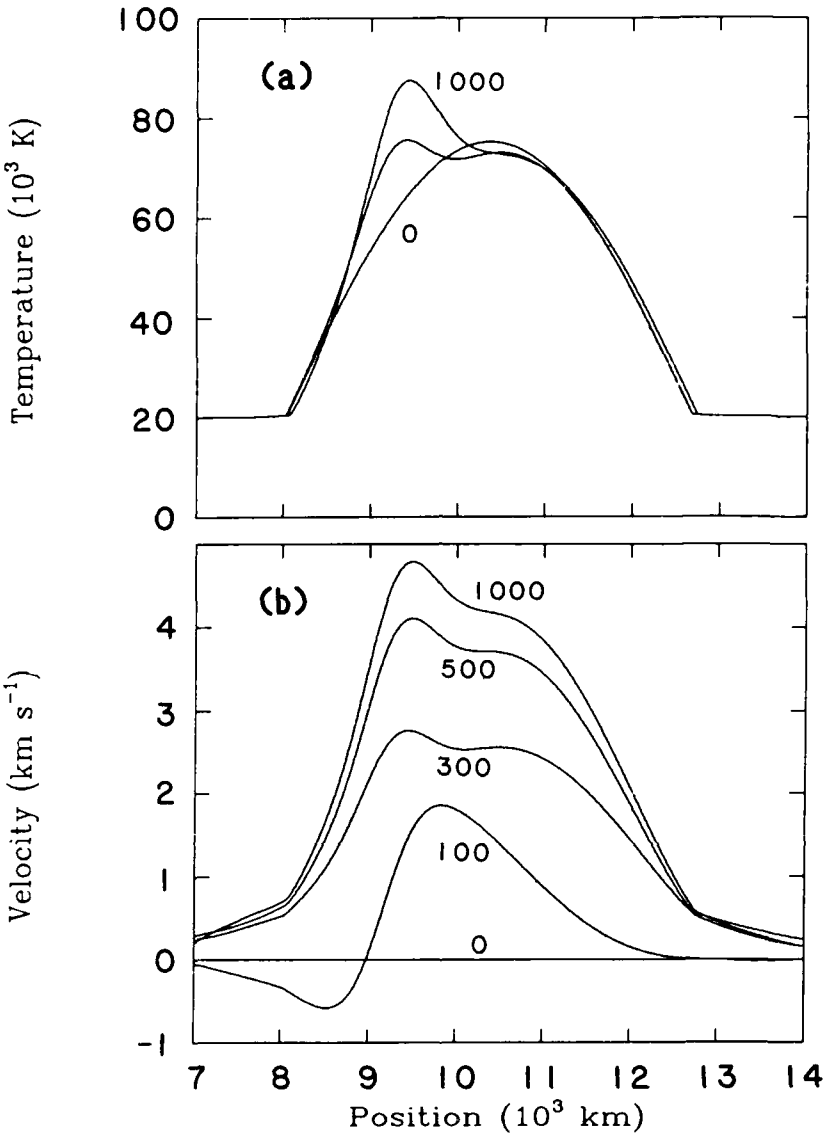

FIG. 2.—The response of the static atmosphere of Fig. 1 to an imposed heating asymmetry: profiles of temperature (*a*) and velocity (*b*) are shown for selected times after a localized energy source has been turned on at position 9.2×10^3 km (half-way up the left leg). Positive velocities are in the direction of increasing position (upflow in the left leg and downflow in the right). The temperature profiles correspond to times of 0, 100, and 1000 s, and the velocity profiles correspond to times of 0, 100, 300, 500, and 1000 s. After 1000 s the atmosphere is essentially unchanged, i.e., steady state.

the other. For a characteristic damping length equal to one-half of the loop length and a magnitude equal to 1.5 times the background heating rate at the left footpoint, the left leg receives nearly twice as much total energy as the right. (Substantially larger differences are not possible without the atmosphere evolving to a hot state.)

As we anticipate on the basis of equation (11), the flow produced by this heating asymmetry is considerably faster than in the previous two cases. Figure 3 shows the beginning, intermediate, and steady state profiles of temperature, velocity, and total number density. The profiles are less structured than in the previous simulations because the energy input varies more slowly with position. Also, the maxima in temperature and velocity now occur on the side of the loop with lesser heating, rather than on the side with greater heating. This occurs because the heating increases with height in the right leg, but decreases with height in the left; temperature gradients must be steeper in the right leg so that radiation can balance the energy input (§ III*a*).

The chromosphere of the final equilibrium is depressed at both the left and right footpoints compared to the initial state. This is understood in terms of the energy balance equation, equation (8), with ϵ taken to be the effective heating rate, including the contribution due to flow terms. Comparing the initial and final states we find that the effective heating rate is increased at both of the footpoints. At the right footpoint, flow heating augments the small increase in mechanical heating, and at the left footpoint, flow cooling is insufficient to offset the

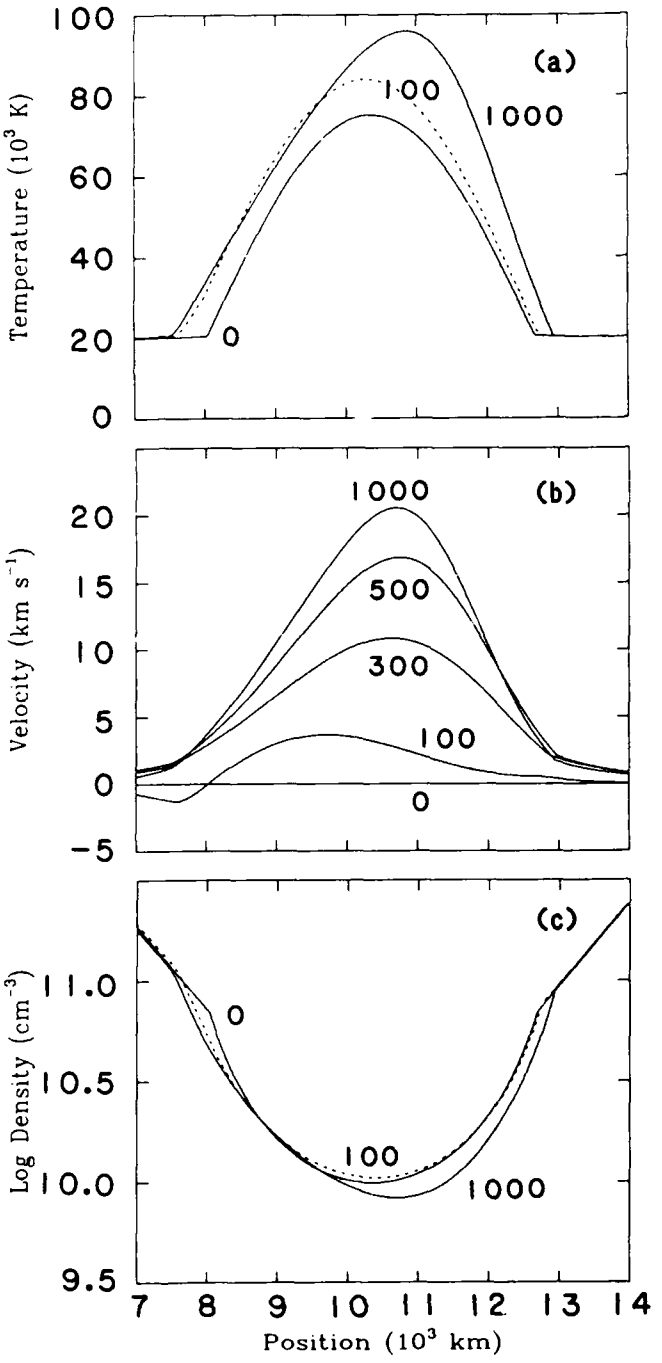

FIG. 3.—The response of the static atmosphere of Fig. 1 to an imposed heating asymmetry: profiles of temperature (*a*), velocity (*b*), and total number density (*c*) are shown for selected times after an energy source has been turned on that decreases exponentially from the left footpoint to the right along the axis of the loop. The temperature and density profiles correspond to times of 0, 100 (*dotted line*), and 1000s, and the velocity profiles correspond to times of 0, 100, 300, 500, and 1000 s. After 1000 s the atmosphere is essentially unchanged, i.e., steady state. Note that the density scale is logarithmic.

large increase in mechanical heating. On both sides the magnitude of the flow term is roughly 50% of the *original* mechanical heating.

Noting that changes in base height are related to changes in base pressure according to $\Delta z_0/H_0 \approx -\Delta P_0/P_0$, we see from equation (8) that

$$\Delta z_0 \gtrsim -\frac{\Delta \epsilon_0}{\epsilon_0}\frac{H_0}{2}, \tag{14}$$

where ϵ_0 is the effective heating and H_0 is the gravitational scale height. For $\Delta\epsilon_0$ positive, Δz_0 is negative and the chromosphere is depressed, as observed in the simulation.

The large velocities of order 20 km s^{-1} in Figure 3 suggest that the net redshifts observed on the Sun may be a result of asymmetric heating of this type. Both downflow and upflow are present, however, and a net redshift will be produced only if the downflowing leg is appreciably faster or appreciably brighter than the upflowing leg. Comparing the velocity and temperature profiles of Figure 3, we see that the downward and upward flow speeds are similar at each temperature. A net redshift is possible, therefore, only if the downflowing leg is relatively bright.

The brightness of an optically thin emission line is proportional to the emission measure, or the square of the electron density integrated over the emitting volume. This emitting volume is, in turn, related to the inverse temperature gradient through the strong dependence of ionization on temperature. As Figure 3 indicates, the steady state densities in the loop are a similar function of temperature in both legs. Differences in emission measure are therefore related to differences in temperature gradient alone.

Since temperature gradients are shallower in the upflowing leg of the loop, we expect that leg to be brighter. This is verified in Figure 4, where we have plotted the emission measures calculated for temperature intervals of 0.3 in the logarithm ($\Delta \log T = 0.3$) at the time of maximum velocity in Figure 3; upflowing and downflowing legs are given separately. The upflows are brighter than the downflows at all but the highest temperatures, where they are comparable. Thus, despite the large velocities, the heating asymmetry considered here is unable to reproduce the net redshifts observed on the Sun. If anything, this simulation would predict a net blueshift.

V. SYMMETRIC HEATING VARIATIONS

We now examine the effects of heating variations that are symmetric about the loop apex. Whereas asymmetric variations produce flows directed from one end of the loop to the other, symmetric variations must produce flows that are of the same sense in both legs, either downward or upward. In general, we expect cooling atmospheres to drain, giving rise to downflows, and heating atmospheres to fill, giving rise to upflows. This is not always the case, however, as we demonstrate shortly.

To study these effects we have performed a series of cooling and heating simulations similar to those performed by Mariska (1987*a*) for hot loops. Beginning with a static atmosphere, we symmetrically reduce the energy input by a prescribed amount over a prescribed period of time. While maintaining this reduced input we then allow the atmosphere to evolve toward the new *static* equilibrium. Once the flows have diminished to well under 1 km s^{-1}, we restore the input to its original level, and the atmosphere returns to its initial state. In this way the loop passes through a complete cycle of cooling and heating. Note that only half the loop need be modeled because of symmetry.

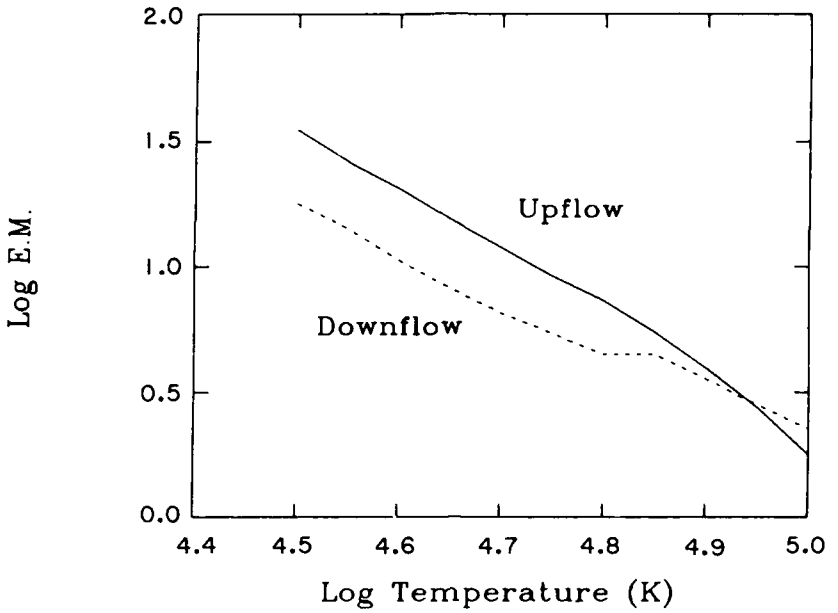

FIG. 4. - Plot of emission measure versus temperature near the time of maximum velocity (1000 s) in the asymmetric heating simulation of Fig. 3. The upflowing (*solid line*) and downflowing (*dotted line*) legs are given separately. The units of emission measure are arbitrary.

a) Short Loop

The relatively short loop we consider first is identical to that used in the previous simulations: its radius of curvature, and therefore height, is 1.5×10^3 km. In the cooling half of the cycle the uniform energy input is everywhere reduced by 90% over a period of 100 s. Figure 5 shows the atmospheric response.

The atmosphere cools quickly, on a time scale that is comparable to the radiative cooling time:

$$\tau_R \sim \frac{4k^2}{(\gamma - 1)\Lambda_0 PT} \sim 200 \text{ s} . \quad (15)$$

This will always be the case as long as the heating is reduced over a time scale that is short compared to the radiative cooling time. If the heating is instead reduced over a longer time scale, the atmosphere will cool at the rate of the reduction itself.

Initially the flow is downward in the loop as the atmosphere collapses from the decrease in thermal support. The chromosphere does not cool, however (because of the isothermal assumption built into the radiative loss curve), and it expands upward into the region of decreasing pressure. During this expansion the chromosphere acts as a snowplow, displacing the hotter material in its way. Before long the entire loop is experiencing an upflow. The greatest velocities occur at the very top of the chromosphere, but at all times they remain slower than 4 km s^{-1}.

Within 2000 s the atmosphere has nearly settled into a new static equilibrium. We then restore the energy input to its original level. The resulting behavior is analogous, but opposite, to before: temperatures and pressures rise in the loop, and the heated plasma expands, forcing the chromosphere downward. After this initial adjustment a small upflow develops as the loop slowly fills with material to regain its original densities.

The maximum downflow of the entire simulation occurs during the cooling phase of the cycle. Because it is so slow, and because it involves lower temperature material, the observed solar redshifts cannot be explained.

b) Tall Loop

For two reasons we expect that a significantly taller loop will respond differently to a similar decrease in heating: first, the chromospheric expansion, which is limited to roughly 1 gravitational scale height according to equation (14), will influence only the lower portion of a tall loop, and second, the material near the top of a tall loop will fall a greater distance and, in principle, should be accelerated to a greater velocity. We have therefore considered a second loop that is 4 times larger than the first. Its radius of curvature is 6×10^3 km.

In order to obtain an initial cool equilibrium in this tall loop it is necessary to assume an energy input that decreases with height; otherwise, only a hot equilibrium is possible (§ III*a*). Instead of prescribing an explicit height dependence, we assume a heating rate that is constant per unit mass and therefore decreases implicitly with height:

$$\epsilon(\rho) \equiv Q_0 \rho , \quad (16)$$

where Q_0 is a constant, set equal to 9.1×10^{10} ergs s^{-1} g^{-1} to achieve a base pressure of 0.2 dyn cm^{-2}.

In the cooling half of the simulation Q_0 is reduced by 90% over a period of 100 s. The loop responds by draining, as indicated in Figure 6. Some initial upflow occurs in front of the expanding chromosphere, but it is quickly overcome by the larger scale downflow. A maximum downward velocity of 17 km s^{-1} is achieved ~ 320 s into the simulation.

This downflow is more than fast enough to explain the solar redshifts; however, because the downward acceleration is so closely linked to cooling, the temperatures must drop substantially before the velocities can become large. This is made clear in Figure 7, where we have plotted velocity versus temperature for three representative times during the simulation. At no time does material hotter than 5×10^4 K exceed a velocity of 5 km

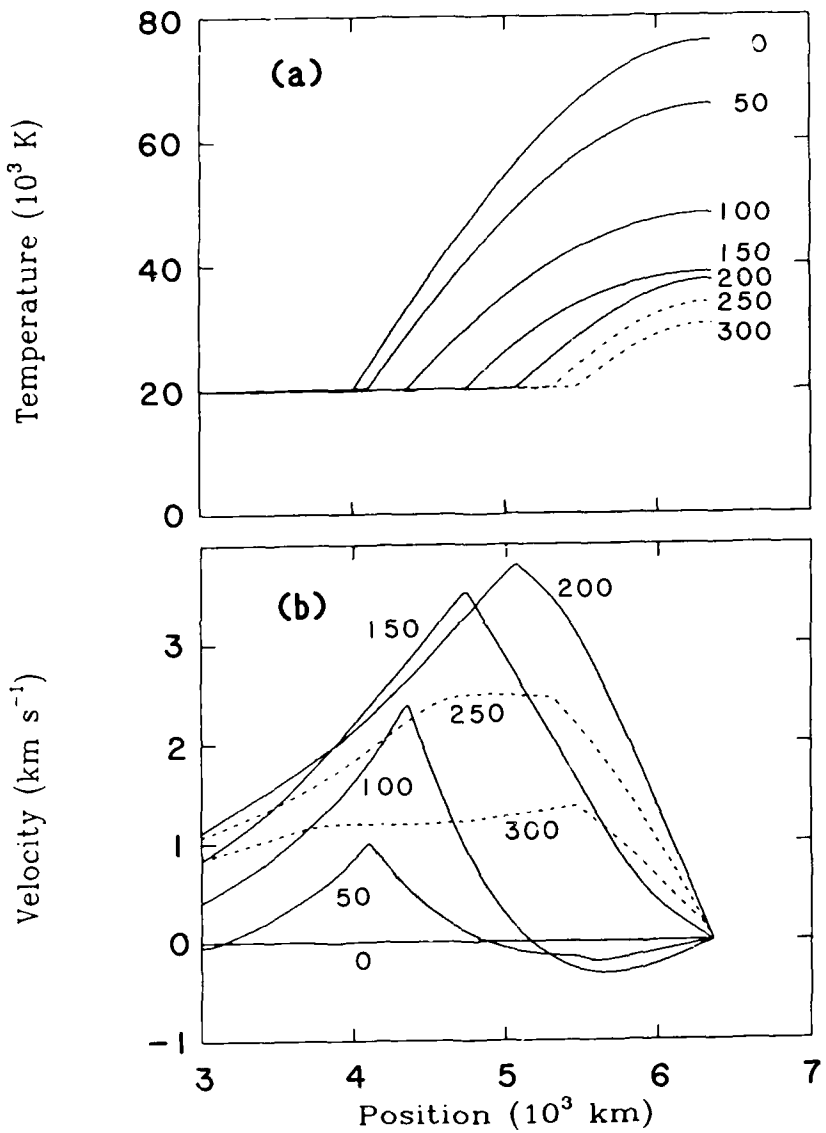

FIG. 5

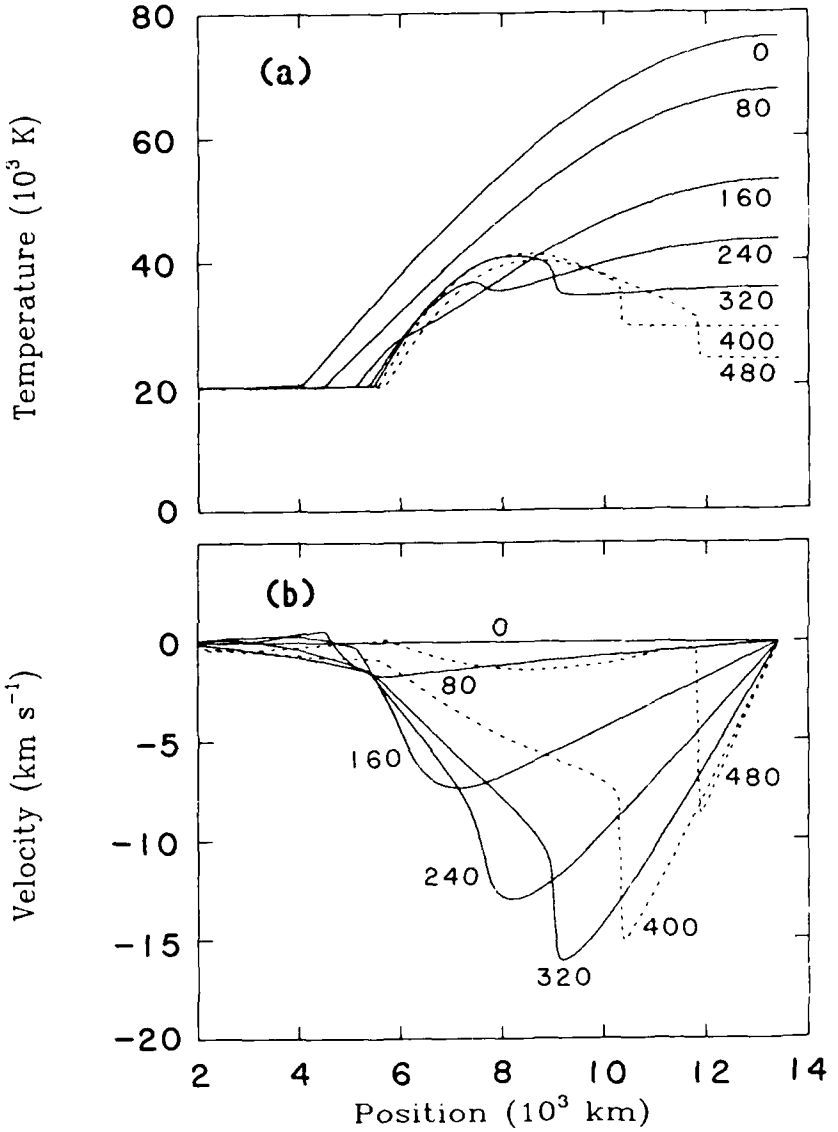

FIG. 6

FIG. 5.—The response of the static short loop atmosphere of Fig. 1 to a uniform reduction in the energy input: profiles of temperature (*a*) and velocity (*b*) are shown for selected times after the 90% heating reduction. Only half of the loop is shown because of symmetry. In both frames the profiles correspond to times of 0, 50, 100, 150, 200, 250, and 300 s. Solid lines indicate conditions before the maximum velocity is reached, and dotted lines indicate conditions afterward.

FIG. 6.—The response of an initially static tall loop atmosphere to a uniform reduction in the energy input: profiles of temperature (*a*) and velocity (*b*) are shown for selected times after the 90% reduction in the heating constant (*see text*). Only half of the loop is shown because of symmetry. In both frames the profiles correspond to times of 0, 80, 160, 240, 320, 400, and 480 s. Solid lines indicate conditions before the maximum velocity is reached, and dotted lines indicate conditions afterward.

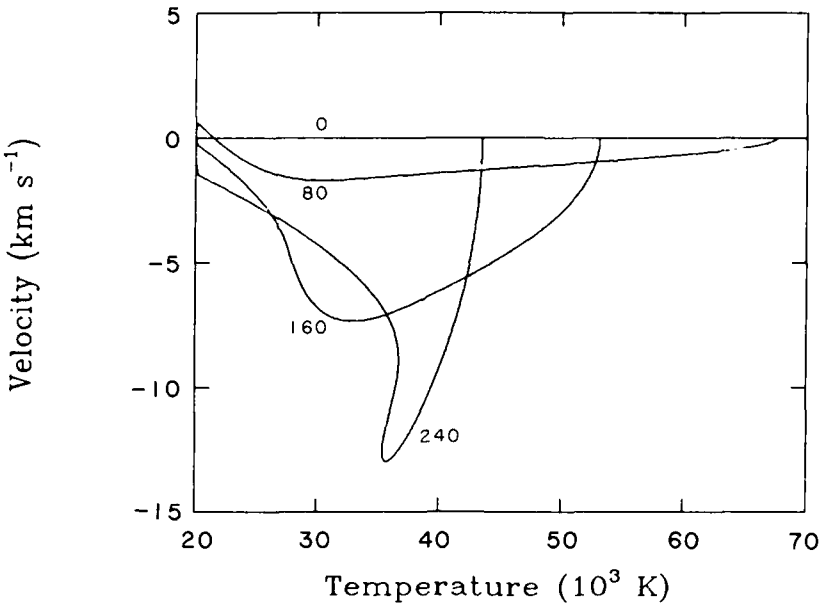

FIG. 7.—Plots of velocity versus temperature at times of 0, 80, 160, and 240 s during the cooling tall loop simulation of Fig. 6.

s^{-1}. Thus, although the downflows are large, they are unable to explain the redshifts observed at temperatures near 10^5 K.

An interesting feature of Figure 6 is the shock that begins to form as the accelerating downflow piles up material in the region above the chromosphere. The Mach number is ~ 0.6 at the last time plotted. As is typically the case, the temperatures are elevated in the region behind the shock front.

In the heating phase of the cycle the behavior is once again analogous, but opposite, to that of the cooling phase. The maximum velocity is upward, at 17 km s^{-1}. Downflows are not significant.

We have performed several other cooling and heating simulations using the same tail loop, but varying both the speed and the degree to which we vary the energy input. As expected, the flow velocities are smaller when the energy input is varied more slowly or when it is varied by a lesser amount. With the heating constant, Q_0, reduced by 90% over a period of 500 s, for example, the maximum velocity is only 6 km s^{-1}. With it reduced by 20% over 100 s, the maximum is 2 km s^{-1}. More rapid reductions in the energy input will have little effect on the flow, since the dynamics of the loop are then limited by the radiative cooling time, which is of order 200 s.

VI. SUMMARY AND DISCUSSION

We have investigated the effects of spatial and temporal variations in the heating of cool loop models in an attempt to explain the net redshifts that are observed on the Sun. In none of the situations we have considered are the induced flows able to satisfactorily reproduce the observations. In the case of asymmetric heating, the end-to-end flows can be as fast as 20 km s^{-1}, but the downflowing leg is neither appreciably faster nor appreciably brighter than the upflowing leg; no net redshift is produced. In the case of symmetric heating, the downflows can also be large, but they are restricted to temperatures that are well below 10^5 K. Neither situation would give rise to the $\gtrsim 7$ km s^{-1} disk-averaged redshifts seen in emission lines of species like C IV.

These results are restricted, of course, by the assumptions of our model. One major assumption is the form of the radiative loss curve, which we have taken to increase as T^3 up to a maximum at 10^5 K. Most of the optically thin loss curves that have been published to date indicate a weaker, $\sim T^2$, dependence between 3×10^4 and 8×10^4 K, although uncertainties in factors such as atomic cross sections and elemental abundances give rise to considerable deviation (Raymond 1979; Cox and Tucker 1969; Pottasch 1965; Summers and McWhirter 1979; Gaetz and Salpeter 1983). The T^3 dependence was proposed originally by McClymont and Canfield (1983) to account for optical depth effects and has been adopted by other investigators (e.g., Antiochos and Noci 1986). Athay (1986*a*) has argued that this is an overcorrection, and so the relevancy of our results may be questioned.

To test the sensitivity of our results to the assumed form of the loss curve we have performed a limited number of asymmetric heating simulations using a loss curve with a $T^{1.5}$ dependence. A background heating that decreases with height is required for the initial static equilibrium; we assume the density-dependent form of equation (16). Under these conditions, we find that cool atmospheres are easily driven to a hot state by even rather small heating asymmetries. In the one cool, steady flow state that was achieved there is not enough difference between the upflowing and downflowing legs to produce a significant Doppler shift. Our conclusion that the observations cannot be explained by spatial variations in the heating is therefore independent of the assumed form of the loss curve, it would seem.

Throughout our calculations we have made the additional assumption that the mechanism responsible for the heating does not impart momentum directly to the atmosphere, i.e., does not exert a force. This may be valid if the heating is a purely local phenomenon (e.g., conversion of magnetic free energy); however, if the heating is due to the dissipation of a wave flux then there is a force associated with the gradient in the wave pressure. In their extensive treatment of the problem, Woods, Holzer, and MacGregor (1987*b*) have shown that, for certain types of waves, this force can be so large as to signifi-

cantly affect the structure of static equilibrium atmospheres. In fact, such equilibria do not always exist when the wave effects are properly taken into account.

To see this, consider the following heuristic description of a wave flux that is incident from below and damped exponentially in the loop:

$$F(s) = F_0 e^{-s/L}, \tag{17}$$

where L is the damping length and F_0 is the flux at the base. The heating and wave pressure (energy density) associated with this flux are

$$\epsilon = -\frac{\partial F}{\partial s} = \frac{F}{L} \tag{18}$$

and

$$P_w = \frac{F}{c}, \tag{19}$$

respectively, where c is the wave speed. The force exerted by the waves is then given by

$$-\frac{\partial P_w}{\partial s} = \frac{\epsilon}{c}\left(1 + \frac{L}{c}\frac{\partial c}{\partial s}\right). \tag{20}$$

For wave speeds that increase with height, as in the case of sound waves or most Alfvén waves, the wave force is necessarily upward with a magnitude of at least ϵ/c. In our models $\epsilon \sim 10^{-2}$ ergs cm^{-3} s^{-1}, and therefore the force due to sound waves would be stronger than the force due to gravity! Alfvén waves would likely exert a weaker force, but their importance depends on the details of the particular model.

The symmetric cooling simulations of § V*b* are unable to reproduce the observed redshifts because in that model the atmosphere is supported solely by thermal pressure gradients; downflows cannot become large until substantial cooling has occurred. If wave pressure effects had been included, the initial atmosphere might have been supported largely by these pressure gradients, and then a reduction in the incident wave flux would allow fast downflows to occur independent of the cooling. Thus, there still remains the possibility that a cooling scenario can explain the solar observations. We hope to explore this further in future simulations that account fully for the existence of waves.

We wish to thank Spiro K. Antiochos and D. Tod Woods for many helpful discussions on the subject of cool loop atmospheres. In addition, we thank Spiro for providing the static equilibria which were the starting point of our time-dependent simulations. This work was sponsored primarily by the Solar Terrestrial Theory Program and the Office of Solar and Heliospheric Physics of the National Aeronautics and Space Administration and by the Office of Naval Research. Numerical simulations were supported by a generous grant of computer time on the NRL Cray XMP from the Director of Research at the Naval Research Laboratory. One of us (J. A. K.) was a National Research Council NRL Cooperative Research Associate and was supported partly by Office of Naval Research Contract N00014-85-K-0111, by NASA Grant NGL05-020-272, and as part of the Solar-A collaboration under NASA Contract NAS8-37334 with Lockheed Palo Alto Research Laboratories.

REFERENCES

Antiochos, S. K. 1984, *Ap. J.*, **280**, 416.
Antiochos, S. K., and Noci, G. 1986, *Ap. J.*, **301**, 440.
Athay, R. G. 1985, *Solar Phys.*, **100**, 257.
———. 1986*a*, *Ap. J.*, **308**, 975.
———. 1986*b*, in *Physics of the Sun*, Vol. 2, *The Solar Atmosphere*, ed. P. A. Sturrock (Boston: Reidel), p. 1.
Athay, R. G., and Holzer, T. E. 1982, *Ap. J.*, **255**, 743.
Book, D. L., Boris, J. P., and Hain, K. 1975, *J. Comp. Phys.*, **18**, 248.
Boris, J. P., and Mariska, J. T. 1982, *Ap. J. (Letters)*, **258**, L49.
Brueckner, G. E. 1981, in *Solar Active Regions*, ed. F. Q. Orrall (Boulder: Colorado Associated University Press), p. 113.
Cox, D. P., and Tucker, W. H. 1969, *Ap. J.*, **157**, 1157.
Craig, I. J. D., and McClymont, A. N. 1986, *Ap. J.*, **307**, 367.
Dere, K. P. 1982, *Solar Phys.*, **77**, 77.
Dere, K. P., Bartoe, J.-D. F., and Brueckner, G. E. 1984, *Ap. J.*, **281**, 870.
———. 1986, *Ap. J.*, **305**, 947.
Doschek, G. A., Feldman, U., and Bohlin, J. D. 1976, *Ap. J. (Letters)*, **205**, L177.
Dowdy, J. F., Jr., Rabin, D., and Moore, R. L. 1986, *Solar Phys.*, **105**, 35.
Feldman, U., Cohen, L., and Doschek, G. A. 1982, *Ap. J.*, **255**, 325.
Gaetz, T. J., and Salpeter, E. E. 1983, *Ap. J. Suppl.*, **52**, 155.
Hood, A. W., and Priest, E. R. 1979, *Astr. Ap.*, **77**, 233.
Klimchuk, J. A. 1986, in *Proceedings of the Solar Prominences and Plasmas Workshop*, ed. A. I. Poland (Greenbelt: NASA GSFC), p. 183.
———. 1987, *Ap. J.*, **323**, 368.
Klimchuk, J. A., Antiochos, S. K., and Mariska, J. T. 1987, *Ap. J.*, **320**, 409.
Klimchuk, J. A., and Mariska, J. T. 1987, *Bull. A.A.S.*, in press.
Mariska, J. T. 1986, *Ann. Rev. Astr. Ap.*, **24**, 23.
———. 1987*a*, *Ap. J.*, **319**, 465.
———. 1987*b*, in *Proceedings of the Fifth Cambridge Workshop on Cool Stars, Stellar Systems, and the Sun*, ed. R. L. Stencel and J. L. Linsky (Berlin: Springer-Verlag), in press.
———. 1987*c*, in preparation.
Mariska, J. T., and Boris, J. P. 1983, *Ap. J.*, **267**, 409.
Mariska, J. T., Boris, J. P., Oran, E. S., Young, T. R., Jr., and Doschek, G. A. 1982, *Ap. J.*, **255**, 783.
Martens, P. C. H., and Kuin, N. P. M. 1982, *Astr. Ap.*, **112**, 366.
McClymont, A. N. 1987, *Bull. A.A.S.*, in press.
McClymont, A. N., and Canfield, R. C. 1983, *Ap. J.*, **265**, 497.
McClymont, A. N., and Craig, I. J. D. 1986, *Nature*, **324**, 128.
———. 1987, *Ap. J.*, **312**, 402.
Pneuman, G. W., and Kopp, R. A. 1978, *Solar Phys.*, **57**, 49.
Pottasch, S. R. 1965, *Bull. Astr. Inst. Netherlands*, **18**, 7.
Raymond, J. C. 1979, private communication.
Rousel-Dupre, D., and Shine, R. A. 1982, *Solar Phys.*, **77**, 329.
Shine, R. A. 1985, private communication.
Summers, and McWhirter, R. W. P. 1979, *J. Phys. B.*, **14**, 2387.
Woods, D. T., Holzer, T. E., and MacGregor, K. B. 1978*a*, in preparation.
———. 1987*b*, in preparation.

JAMES A. KLIMCHUK: Center for Space Science and Astrophysics, Stanford University, ERL 300, Stanford, CA 94305

JOHN T. MARISKA: Code 4175, Naval Research Laboratory, Washington, DC 20375